

Band-width control in a perovskite-type $3d^1$ correlated metal $\text{Ca}_{1-x}\text{Sr}_x\text{VO}_3$. I. Evolution of the electronic properties and effective mass.

I. H. Inoue^{*,†}

Precursory Research for Embryonic Science and Technology, Japan Science and Technology Corporation,
and Electrotechnical Laboratory, 1-1-4 Umezono, Tsukuba 305, Japan

O. Goto

Department of Electronics and Communications, Meiji University, 1-1-1 Higashi-Mita, Tama-ku, Kawasaki 214, Japan

H. Makino

Institute of Applied Physics, University of Tsukuba, 1-1-1 Tennodai, Tsukuba 305, Japan

N. E. Hussey[‡]

Interdisciplinary Research Centre in Superconductivity, University of Cambridge, Madingley Road, Cambridge CB3 0HE,
United Kingdom

M. Ishikawa

Institute for Solid State Physics, University of Tokyo, 7-22-1 Roppongi, Minato-ku, Tokyo 106, Japan

December 25, 1997

Single crystals of the perovskite-type $3d^1$ metallic alloy system $\text{Ca}_{1-x}\text{Sr}_x\text{VO}_3$ were synthesized in order to investigate metallic properties near the Mott transition. The substitution of a Ca^{2+} ion for a Sr^{2+} ion reduces the band width W due to a buckling of the V-O-V bond angle from $\sim 180^\circ$ for SrVO_3 to $\sim 160^\circ$ for CaVO_3 . Thus, the value of W can be systematically controlled without changing the number of electrons making $\text{Ca}_{1-x}\text{Sr}_x\text{VO}_3$: one of the most ideal systems for studying band-width effects. The Sommerfeld-Wilson's ratio ($\simeq 2$), the Kadowaki-Woods ratio (in the same region as heavy Fermion systems), and a large T^2 term in the electric resistivity, even at 300 K, substantiate a large electron correlation in this system, though the effective mass, obtained by thermodynamic and magnetic measurements, shows only a systematic but moderate increase in going from SrVO_3 to CaVO_3 , in contrast to the critical enhancement expected from the Brinkmann-Rice picture. It is proposed that the metallic properties observed in this system near the Mott transition can be explained by considering the effect of a non-local electron correlation.

PACS number(s): 71.28.+d, 71.30.+h, 71.20.Be

I. INTRODUCTION

Despite extensive investigations on $3d$ transition-metal (TM) oxides,¹ there remain many more mysteries still to unravel. The discoveries of metal-to-insulator transitions (MIT) in $3d$ TM oxides with a partially filled $3d$ band, for example, has given us great incentive to re-examine several previous studies of the electronic states in these TM oxides.

The most important feature of this kind of $3d$ TM oxides is that simple one-electron band theory is no longer sufficient to give a good account of the electronic states, since the electron correlations are much larger than expected for the one-electron band-width.² Mott first introduced the concept of MIT caused by a strong Coulomb repulsion of electrons.³ Although the description of the MIT (Mott transition) is still argued from various points of view,⁴ a more challenging problem lies in the metallic phase near the Mott transition, where a narrow-band

system is known to show *anomalous* metallic properties, and substantial enhancement of the fluctuations of spin, charge and orbital correlations is observed. This problem has been investigated with renewed vigor since the discovery of high- T_c cuprate superconductors and although a number of enlightening works have been done so far, still we cannot grasp a comprehensive view of the whole physics.

As one of the open questions, in this paper, we focus on the problem of the effective mass in the perovskite-type $3d^1$ correlated metal $\text{Ca}_{1-x}\text{Sr}_x\text{VO}_3$. An important manifestation of the mass enhancement in the perovskite-type light- $3d$ TM oxides has been given by Tokura *et al.*⁵ They reported filling-dependent electronic properties in the $\text{Sr}_{1-x}\text{La}_x\text{TiO}_3$ system near the MI transition around $x = 1$. The LaTiO_3 ($x = 1$) material behaves as an insulator below 300 K and antiferromagnetic ordering of Ti $S = 1/2$ spins occurs at $T_N = 120 \sim 150$ K.⁶ They also reported that Fermi-liquid-like behavior was observed even in the immediate vicinity of the MI phase

boundary, with a critical increase of m^* arising from the effect of the enhanced electron correlations. Within the framework of Fermi-liquid theory, the only way to approach MIT continuously is to realize the divergence of the single-quasi-particle mass m^* at the MIT point.⁷ The critical behaviors observed in the $\text{Sr}_{1-x}\text{La}_x\text{TiO}_3$ system are fairly systematic, thus provoking intense theoretical study; however there is still room for arguments, especially in the following points:

1. Tokura *et al.* compared the effective mass m^* to the free electron mass m_0 . However, the x -dependence of the “band-mass” m_b should also be taken into account. Compared with the value of m_b for the similar system CaVO_3 , the mass enhancement of the $\text{Sr}_{1-x}\text{La}_x\text{TiO}_3$ system is not so large, except for the region $x > 0.95$.
2. The critical increase of the value of m^* in the $\text{Sr}_{1-x}\text{La}_x\text{TiO}_3$ system is only seen in the region very close to MI transition boundary.⁸ However, in this region, it is not obvious whether Fermi-liquid theory is still valid. In fact, in the region of significant mass-enhancement ($x > 0.95$), the number of carriers are actually depleted.⁸
3. Another filling-dependent MI transition is observed in the $\text{Y}_{1-x}\text{Ca}_x\text{TiO}_3$ system.^{9,10} However MIT occurs around $x = 0.4$ which is relatively far from integral filling. Nevertheless, the effective mass shows a conspicuous enhancement in the vicinity of MIT similar to that seen in the $\text{Sr}_{1-x}\text{La}_x\text{TiO}_3$ system. Thus, it seems reasonable to suppose that this kind of mass-enhancement, observed in those “filling-control” systems close to MIT, might be induced by fluctuations or inhomogeneity of the insulating phase near the boundary of MIT.

The above problems can be due to the fact that the critical behaviors depend on a path along which a system approaches the boundary of MIT. In the $\text{Sr}_{1-x}\text{La}_x\text{TiO}_3$ system, the band-filling is dominantly controlled instead of the band-width.

The question then arises; how does the effective mass in the metallic state actually change as we change solely the electron correlation without changing the band-filling? In order to elucidate this issue, another type of systematic experiment is required; *i.e.*, we need to control only the $3d$ band width W in a particular system while keeping the number of carriers fixed.

Representative examples are the pressure-induced MIT reported in V_2O_3 ,¹¹ where hydrostatic pressure modifies W . However, for a quantitative discussion, we need to know the change of the lattice constants under pressure. Moreover, in general, the anisotropic compressibility due to the anisotropy of the lattice structure affects W in a complex manner. Other examples are found in nickel-based compounds: the perovskite-type $R\text{NiO}_3$ with R of the trivalent rare-earth ions (La to Lu),¹² and the pyrite-type chalcogenide system $\text{NiS}_{2-x}\text{Se}_x$.¹³ Since the insulating state of these nickel compounds is classified as a

charge-transfer insulator rather than a Mott-Hubbard insulator in the so-called Zaanen-Sawatzky-Allen classification scheme of TM compounds.^{14,15} Therefore, MIT occurs as a closing of the charge-transfer gap with increase of the p - d hybridization. Thus, it is inevitable that MIT is not described by the simple model of the Mott transition and the metallic state is more complicated.

Based on these considerations, we have synthesized a solid solution of the perovskite-type metallic vanadates, CaVO_3 and SrVO_3 , in order to investigate the metallic state near the Mott transition more simply with a systematic band-width control. We have succeeded in obtaining single crystals of the homogeneous metallic alloy system $\text{Ca}_{1-x}\text{Sr}_x\text{VO}_3$ with nominally one $3d$ electron per vanadium ion. In the $\text{Ca}_{1-x}\text{Sr}_x\text{VO}_3$ system, as we isovalently substitute a Ca^{2+} ion for a Sr^{2+} ion, a lattice distortion occurs. This is governed by the so-called tolerance factor f of the perovskite-type compounds ABO_3 defined as

$$f = \frac{R_A + R_O}{\sqrt{2}(R_B + R_O)},$$

where R_A , R_O , and R_B are the ionic radii of the A ion, the O ion (oxygen), and the B ion, respectively. When the value of f is almost 1, the system is cubic; while for $f < 1$, the lattice structure changes to rhombohedral and then to the orthorhombic GdFeO_3 type. In the GdFeO_3 structure, it is known that the B-O-B bond angle decreases continuously with decreasing f almost irrespectively of the set of A and B.¹⁶ According to the literature,¹⁷ the ionic radii of Ca^{2+} , Sr^{2+} , V^{4+} , and O^{2-} ions are 1.34, 1.44, 0.58, and 1.40 Å, respectively. Thus we obtain a value of f of 1.014 for SrVO_3 , and 0.979 for CaVO_3 , corresponding to a V-O-V bond angle of $\sim 180^\circ$ for SrVO_3 and $\sim 160^\circ$ for CaVO_3 . The buckling of the V-O-V bond angle reduces the one-electron $3d$ -band width W , since the effective 3d-electron transfer interaction between the neighboring V-sites is governed by the supertransfer process via the O $2p$ state.

Thus, the ratio of the electron correlation U normalized to W (U is considered to be kept almost constant by the substitution) can be systematically controlled in $\text{Ca}_{1-x}\text{Sr}_x\text{VO}_3$ without varying the nominal carrier concentration. Furthermore, the V-O-V bond angle of CaVO_3 ($\sim 160^\circ$) is almost equal to insulating LaTiO_3 , so it is reasonable to consider that CaVO_3 is close to the MIT boundary and thus is an ideal system for the investigation of the metallic state near the Mott transition.¹⁸ In fact, some spectroscopic manifestation of the strong electron correlation has been reported already,¹⁹⁻²² showing that there is significant spectral weight redistribution in the $\text{Ca}_{1-x}\text{Sr}_x\text{VO}_3$ system. Therefore, the effective mass of this system, especially at the $x = 0$ end (CaVO_3), is expected to be enhanced as discussed for $\text{Sr}_{1-x}\text{La}_x\text{TiO}_3$ near the insulating composition LaTiO_3 .

Nevertheless, the $\text{Ca}_{1-x}\text{Sr}_x\text{VO}_3$ system does *not* show such a significant enhancement of the effective mass. The goal of this paper is to reveal intriguing behavior in the evolution of the effective mass, as we control the U/W

ratio in this system. Details of the experiments, especially the method of preparing single crystals of this new vanadate system, are described in Sec. II. We discuss the cubic-orthorhombic lattice distortion in Sec. IIIA. The results from magnetic susceptibility measurements and the obtained effective mass m^* are shown in Sec. IIIB, and compared to m^* deduced from the electronic specific heat coefficient in Sec. IIIC. The Sommerfeld-Wilson's ratio is found to be almost equal to 2, that is strong evidence of the large electron correlation. The electric resistivity data are analyzed by a model incorporating the electron-electron interaction (T^2 term) as well as the electron-phonon interaction (Bloch-Grüneisen term) in Sec. IIID. It is noted that the Kadowaki-Woods ratio lies in the same region as the heavy Fermion compounds. Finally, we discuss the effect of non-local electron correlations, *i.e.*, the momentum-dependent self-energy, which can be significant near the Mott transition, in order to explain consistently both the strong electron-correlations and the missing enhancement of the effective mass.

II. EXPERIMENTAL

A ‘ceramic method’ was employed in order to prepare poly-crystalline samples. 4N CaCO_3 , SrCO_3 and VO_2 were used as starting reagents. We prepared CaO and dried SrCO_3 by pre-heating both the CaCO_3 and SrCO_3 compounds in air for 24 hours at 1000°C , and weighed the powders while they were still over 100°C . We confirmed that the dried CaO and SrCO_3 , as well as VO_2 , were all single phase by x-ray diffraction (XRD). The starting compounds, CaO , SrCO_3 , and VO_2 were then mixed in the required molar ratio $\text{Ca} : \text{Sr} : \text{V} = 1 - x : x : 1$ and then calcined several times at 1250°C in flowing argon atmosphere ($\sim 1000 \text{ cc/min}$) with intermittent grindings. Because the reaction proceeds in the solid state, the reaction rate depends on the diffusion rate of the constituents through the product phases. As the reaction proceeds, diffusion paths become longer, and hence the reaction rate decreases. Therefore the intermittent mechanical grinding of the reaction product is important in this method.

As the Sr concentration is increased, it is required to add hydrogen-gas at a rate up to $\sim 50 \text{ cc/min}$. The amount of hydrogen-gas flow for each calcination process must be controlled in order to avoid too much reduction and peroxidation. The amount of the oxidation was conveniently checked by examining the XRD spectrum, *i.e.* the lattice constants, of the reaction product every time after the intermittent grinding. This process was repeated until completion of the reaction.

Finally, the powder was put into rubber tubes and each tube was pressed under hydrostatic pressure of 1000 atm to form a cylindrical rod of $\sim 6 \text{ mm}$ diameter and $\sim 10 \text{ cm}$ length. The rods were sintered at 1300°C in the same atmosphere described above.

Single crystals of $\text{Ca}_{1-x}\text{Sr}_x\text{VO}_3$ were grown by the floating zone (FZ) method in an infrared-radiation furnace (Type SC-N35HD, Nichiden Machinery Ltd.) with

two 1.5 kW halogen lamps as radiation sources. At first, the sintered rod is cut into two parts: one is $\sim 2 \text{ cm}$ long for the “seed” rod, which is held at the top of the lower-shaft, and the rest of the sintered rod, called the “feed” rod, is suspended at the bottom of the upper-shaft. Each rod is rotated at $\sim 20 \text{ rpm}$ in opposite directions. The lamp power is raised gradually until both the rods are melted, then the molten zone is attached to the top of the seed. The molten zone is passed through the whole feed rod at a rate of $\sim 1 \text{ cm/hour}$ in flowing argon atmosphere without any interruption or change of lamp power. The most important point here is to control the reduction atmosphere delicately, depending on the amount of the Sr content x , and also on the oxygen stoichiometry of the feed rod. As we increase the value of x , it is necessary to add $< 0.1\%$ hydrogen to the flowing argon. As soon as this small amount of hydrogen is added, however, the melting temperature rises drastically, and the molten zone shrinks unless we increase the lamp power once more. On the other hand, if the amount of hydrogen gas is not sufficient, the liquid phase in the molten zone loses viscosity and spills by degrees along the rod. Furthermore, a different phase, which might be a peroxidized phase, appears in the molten zone and precipitates on the surface of the zone to form an “antler”. Thus, a delicate feed-back control of the amount of hydrogen gas and the power of the halogen lamp is necessary to obtain a single crystal with sufficient quality. Typical dimensions of a single-crystalline grain in the resultant rods are $\sim 2 \times 1 \times 1 \text{ mm}^3$.

Each crystal was examined by powder XRD and by Laue photography to check for homogeneity. Results are summarized in the next section.

The oxygen off-stoichiometry in $\text{Ca}_{1-x}\text{Sr}_x\text{VO}_3$ was determined using a Perkin-Elmer TGA-7 thermogravimetric (TG) analyzer from the weight gain on heating the sample to around 1300 K in flowing air and assuming that the final oxidation state of a vanadium ion was $+5$. Neither weight gain due to peroxidation, nor weight loss due to desorption of the oxygen was observed, once the highest-oxidized material $(\text{Ca}_{1-x}\text{Sr}_x)_2\text{V}_2\text{O}_7$ was obtained.

As-prepared samples contain a certain amount of oxygen defects. The result of the TG measurements indicated that, with increasing temperature, the samples are abruptly oxidized at around 420 K .²³ Moreover, after this oxidation, the oxygen concentration of the samples becomes stoichiometric and no further oxidation occurs until the temperature reaches around 700 K . Therefore, we were able to prepare samples without any oxygen off-stoichiometry by annealing the samples in air at $\sim 200^\circ\text{C}$ for around 24 hours.

The stoichiometry of the ratio $\text{Ca} : \text{Sr} : \text{V} = 1 - x : x : 1$ was confirmed by an inductively coupled plasma atomic emission spectrometer (SEICO, SPS7000). The amount of off-stoichiometry in the single-crystalline samples was within the error bar, *i.e.*, less than 1%.

In order to perform the dc-electric resistivity measurement, the single crystalline samples were cut and shaped

into rectangular parallelepipeds without particular attention to the alignment of the crystal axes. A typical example of the dimension of the parallelepiped was $2 \times 0.5 \times 0.3 \text{ mm}^3$. We also prepared samples with two different alignments: for one set of samples, the longest-edge, along which the measuring current flows, is parallel to the [100]-axis of the pseudocubic perovskite, and for the other set, the current flows along the [110]-axis. Some of these samples showed clear dependence on the alignment. However, this was not due to any features in the electronic structure as discussed in the following section. All the electric resistivity measurements were done with a standard dc four-terminal method. Four copper leads ($50 \mu\text{m}\phi$) were attached with silver paste (Du Pont 4922). The measuring current was typically $\pm 15 \text{ mA}$ supplied by a constant current source. Since the $x = 1$ sample was much smaller than the other ones, we measured its resistivity using the Van der Pauw technique in which one places the contacts on the corners and rotates the current and voltage configuration. The data were collected on both heating and cooling cycles.

dc-susceptibility measurements were performed using a commercial rf-SQUID magnetometer (Quantum Design, MPMS-II) without particular attention to the alignment of the crystal axes. The measuring field was calibrated up to 5 Tesla with a Pd standard.

Specific heat data were obtained on polycrystalline samples²⁴ between ~ 0.5 and $\sim 20 \text{ K}$ using a semi-adiabatic heat-pulse method.²⁵

III. RESULTS AND DISCUSSION

A. Lattice constants

The XRD patterns of $\text{Ca}_{1-x}\text{Sr}_x\text{VO}_3$ for varying Sr content are displayed in Fig. 1 and the deduced lattice parameters are shown in Fig. 2. The lattice pa-

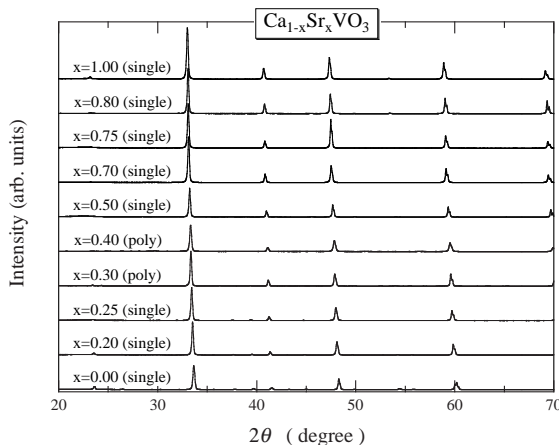


FIG. 1. X-ray powder diffraction patterns of single-crystalline $\text{Ca}_{1-x}\text{Sr}_x\text{VO}_3$ at room temperature. $x = 0.3$ and $x = 0.4$ samples are poly crystals.

rameters change systematically from the orthorhombic CaVO_3 to SrVO_3 which is simple-cubic within the error bar ($\sim \pm 0.2\%$). According to the four-axes XRD

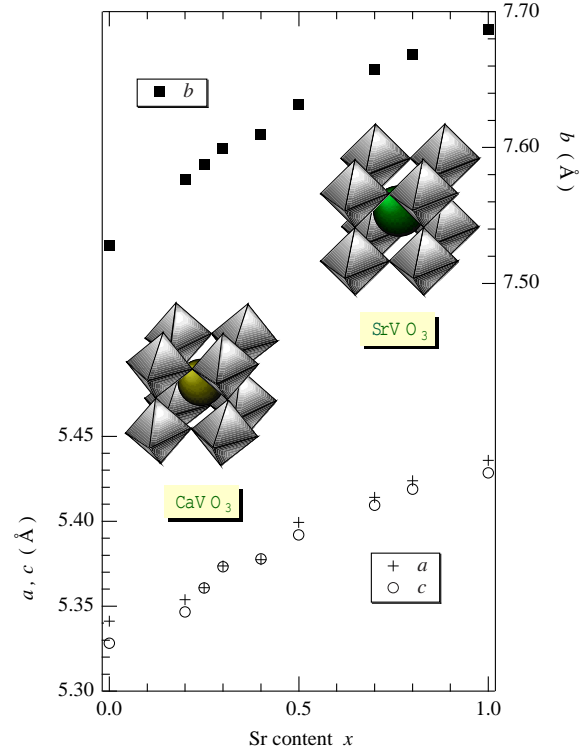


FIG. 2. The lattice parameters a , b , and c of $\text{Ca}_{1-x}\text{Sr}_x\text{VO}_3$ at room temperature, estimated from the XRD patterns. The data are plotted against Sr content x . Note that each deduced lattice parameter contains around $\pm 0.2\%$ error. Thus it is not appropriate to discuss the exact crystal symmetry based only on this plot.

measurement,²⁶ the lattice constants of CaVO_3 are $a = 0.53185(8) \text{ nm}$, $b = 0.7543(2) \text{ nm}$, and $c = 0.53433(8) \text{ nm}$. The V-O-V bond-angle is $154.(3)^\circ$ for V ions on the ac-plane (V-O bond length is $0.1891(6) \text{ nm}$) and $171.(0)^\circ$ for V ions along the b-axis (V-O bond lengths are $0.190(0) \text{ nm}$ and $0.196(5) \text{ nm}$).²⁶ This large buckling of the V-O-V bond angle ($\sim 160^\circ$ in average) is considered to make the one-electron $3d$ band-width W of this system smaller than that of SrVO_3 , where the V-O-V bond angle is almost exactly 180° .

B. Magnetization

Figure 3 shows the temperature-dependence of the magnetic susceptibilities χ of $\text{Ca}_{1-x}\text{Sr}_x\text{VO}_3$ at $5 \text{ Tesla} \equiv 50000 \text{ Oe}$. Since none of the samples showed any significant hysteresis between the heating and cooling cycles, we have plotted data for the heating process only.

The field-dependence of the magnetization M of SrVO_3 is plotted in Fig. 4. We measured M up to 5 Tesla while increasing and decreasing the applied field H at both 5 K and 300 K. At 300 K, the magnetization curve shows no hysteresis and M depends linearly on H . This means that only paramagnetic moments contribute to the total magnetization. When we decrease the temperature to 5 K, the magnetization curves become hysteretic and also

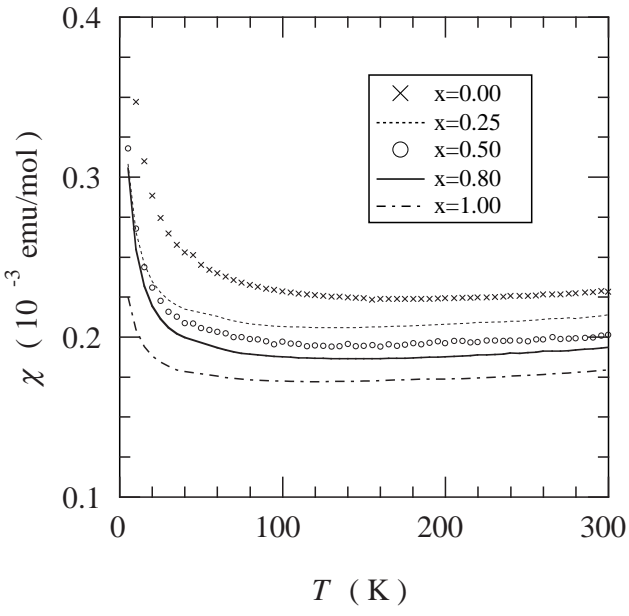


FIG. 3. Magnetic susceptibilities χ of single-crystalline $\text{Ca}_{1-x}\text{Sr}_x\text{VO}_3$ for $x = 0.00, 0.25, 0.50, 0.80$, and 1.00 measured at $5\text{ Tesla} \equiv 50000\text{ Oe}$ plotted against temperature T . Samples were cooled to 4 K with no applied field and then warmed up to 300 K in 5 Tesla . No significant hysteresis was observed during the heating and cooling cycles.

show a slight upturn.

Here we note that in perovskite-type oxides with the formula ABO_3 , oxygen and A/B stoichiometries are fairly unstable. The off-stoichiometry is not accidental but characteristic of these compounds. Even though one tries to obtain sufficiently stoichiometric compounds in ABO_3 materials within experimental requirements, the off-stoichiometry is still present intrinsically and such inevitable defects are called “native-defects” to indicate

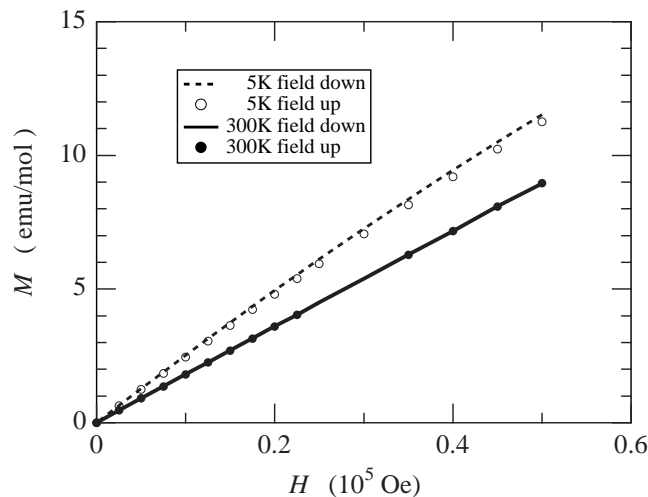


FIG. 4. Magnetization M of SrVO_3 plotted against the applied field H . The data were collected while increasing and decreasing the applied field between 0 to 5 Tesla at both 5 K and 300 K .

that their properties are reproducible.²⁷ We have so far reported the effects of the (unavoidable) oxygen off-stoichiometry in CaVO_3 by intentionally introducing the oxygen defects in varying degrees.^{23,28,29} In this study, although we tried to prepare oxygen-stoichiometric samples using a delicate annealing procedure, there still exists a very small but irreducible amount of inevitable oxygen defects.

Local moments due to these oxygen defects contribute to M as a spontaneous magnetization or in this case a sublattice magnetization, because the Weiss temperature is negative. The value of M is very small compared with that observed in $\text{CaVO}_{2.8}$ ²⁹ and is consistent with the number of local moments deduced from the Curie constants (*vide infra*).

All the magnetic susceptibility data χ are well reproduced by the following formula:

$$\chi_P + \chi_{dia} + \chi_{core} + \chi_{orb} + \frac{C}{T - \vartheta} + \alpha T^2, \quad (1)$$

where χ_P is the Pauli paramagnetic term, χ_{dia} is the Landau diamagnetization, χ_{core} comes from the diamagnetic contribution of the core-levels, and χ_{orb} is due to the orbital paramagnetization. The Curie-Weiss term is attributed to impurities such as the native oxygen defects.

The last term is considered to originate from the higher-order temperature-dependent term in the Pauli paramagnetism, that is neglected in the zeroth order approximation, and reflects the shape of the density of states (DOS) $D(\omega)$ $\text{erg}^{-1}\text{cm}^{-3}$ at the Fermi energy E_F . Both the first and the last terms can be expressed together as

$$\begin{aligned} \chi_P(T) &= \sum_{\vec{k}, n} \left(\frac{\partial \varepsilon_n(\vec{k})}{\partial H} \Big|_{H=0} \right)^2 \delta(E_F - \varepsilon_n(\vec{k})) \\ &= \frac{\chi_P^0(T)}{1 - \alpha \chi_P^0(T)}, \end{aligned}$$

where

$$\begin{aligned} \chi_P^0(T) &= \chi_P^0(0)(1 + cT^2), \\ \chi_P^0(0) &= 2\mu_B^2 D(E_F), \\ c &= \frac{(\pi k_B)^2}{6} \frac{d^2 \ln D(\varepsilon)}{d\varepsilon^2} \Big|_{\varepsilon=E_F}, \end{aligned}$$

$\varepsilon_n(\vec{k})$ is the one-electron energy of the eigenstate, c can be either negative or positive depending on the shape of DOS at E_F , and $\mu_B = 9.274 \times 10^{-21} \text{ erg Oe}^{-1}$.

The first two terms are re-written using the effective mass m^* and the bare band mass m_b of the system [we employ m_b deduced from the band calculation using a local density approximation (LDA),³⁰ rather than m_b of the non-interacting Bloch electrons]:

$$\begin{aligned} \chi_{spin} &= \chi_P + \chi_{dia} \\ &= \left(\frac{m^*}{m_b} - \frac{m_b}{3m^*} \right) \chi_P^{LDA}, \end{aligned} \quad (2)$$

where χ_P^{LDA} stands for the Pauli paramagnetic term deduced from the LDA band calculation:

$$\chi_P^{LDA} [\text{emu/mol} \equiv \text{erg Oe}^{-2} \text{mol}^{-1}] = N v \mu_B^2 D(E_F)$$

where $N \text{ mol}^{-1}$ is the number of itinerant electrons per one mole of unit formula and $v \text{ cm}^3$ is the volume of the unit formula. For $D(E_F)$, a simple correction has been done by multiplying the value of $1/\cos^2(\angle \text{V-O-V})$ to the bare LDA DOS at E_F in order to account for the narrowing of the band due to the buckling.

For the third term χ_{core} , we have used the values given in the literature,³¹ as summarized in Table I.

TABLE I. Core diamagnetism of the constituent ions in $\text{Ca}_{1-x}\text{Sr}_x\text{VO}_3$.³¹

ion	χ_{dia} emu/mol
Ca^{2+}	-13.3×10^{-6}
Sr^{2+}	-28.0×10^{-6}
V^{5+}	-7.7×10^{-6}
O^{2-}	-12.6×10^{-6}

The fourth term is

$$\begin{aligned} \chi_{orb} &= - \sum_{\vec{k}, n} \frac{\partial^2 \varepsilon_n(\vec{k})}{\partial H^2} \bigg|_{H=0} \theta(E_F - \varepsilon_n(\vec{k})) \\ &= 2\mu_B^2 \sum_{n, n'} \sum_{\mu} \int \frac{d\vec{k}}{(2\pi)^3} \frac{|\langle n\vec{k}|l_{\mu z}|n'\vec{k}\rangle|^2}{\varepsilon_{n'}(\vec{k}) - \varepsilon_n(\vec{k})} \\ &\quad \times (f(\varepsilon_n) - f(\varepsilon_{n'})), \end{aligned}$$

where $l_{\mu z}$ is the z -component of the orbital angular momentum \vec{l}_{μ} ($\mu = 1, \dots, 5$) for the d -orbital, and $f(x)$ is the Fermi-Dirac distribution function. This term corresponds to the Van Vleck paramagnetism in insulating materials, and becomes large when the “quenching” of the orbital angular moment is not sufficient. Moreover, it has been suggested that this term can also be enhanced by the electron correlation, since electron correlations change the electron configuration as well as the crystal field, and the Van Vleck term cannot be treated by a one-body approximation.³² This is still a difficult question; for this system, we used an x -independent value of $\chi_{orb} = 6.5 \times 10^{-5}$ emu/mol estimated in another $3d^1$ metallic vanadate system VO_2 .³³ Hence, we can fit Eq. 1 to the observed data.

The obtained values of the Curie-Weiss term C are as small as $0.5 \sim 2.2 \times 10^{-3}$ emu K/mol, and the Weiss temperatures $\theta = -6.0 \sim 1.6$ K, indicating very weak antiferromagnetic interaction among the local moments. These small values of the Curie-Weiss term are considered to be due to the V^{3+} ($S = 1$) local impurity moment arising from the “native oxygen defects”. From the value of $C = 2.2186 \times 10^{-3}$ emu K/mol for CaVO_3 , we can evaluate that only 0.22% of the V sites have the $S = 1$ local moment; this amount of local impurities

TABLE II. The effective mass deduced from the fit to the magnetic susceptibility data with Eq. 1 and Eq. 2, where χ_{core} and χ_{orb} are fixed to the values in the literature.^{31,33} χ_P^{LDA} are calculated from $D(E_F)$ obtained by the LDA band calculation³⁰ multiplied by $\cos^{-2}(\angle \text{V-O-V})$ which accounts for the narrowing of the band due to the buckling.

x	χ_{spin} (emu/mol)	χ_P^{LDA} (emu/mol)	m^*/m_b
0.00	2.008×10^{-4}	6.137×10^{-5}	3.273
0.20	1.905×10^{-4}	6.046×10^{-5}	3.202
0.25	1.904×10^{-4}	6.022×10^{-5}	3.223
0.50	1.788×10^{-4}	5.907×10^{-5}	3.153
0.70	1.678×10^{-4}	5.815×10^{-5}	3.064
0.80	1.678×10^{-4}	5.769×10^{-5}	3.112
1.00	1.606×10^{-4}	5.677×10^{-5}	3.087

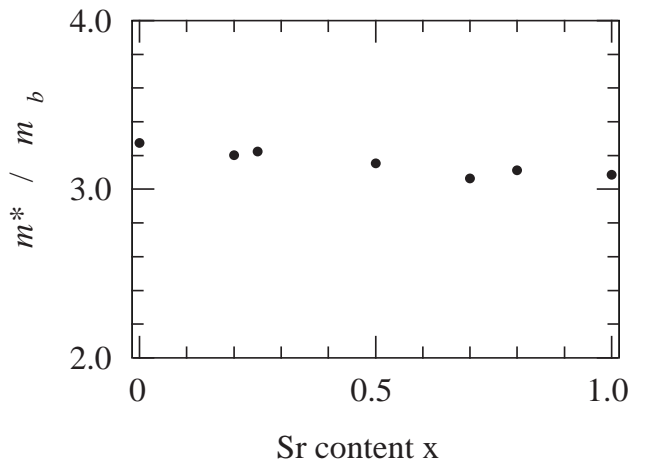


FIG. 5. Effective mass m^* compared with the LDA band mass m_b plotted against Sr content x . m^*/m_b increases systematically in going from SrVO_3 to CaVO_3 . The values are not as large as expected.

is inevitable in ABO_3 materials, but irrelevant for our discussion of the metallic properties, such as the value of the effective mass. The obtained values of the coefficient α of the last term in Eq. 1 are also very small ($0.5 \sim 2.5 \times 10^{-10}$ emu K $^{-2}$ mol $^{-1}$). This means that the deviation from a temperature-independent Pauli paramagnetism is fairly small in the temperature range we measured. Only when we need to estimate the value of m^* from χ_P much more accurately will it be necessary to perform the measurement up to higher temperatures.

The obtained ratio of the effective mass m^* to the LDA band mass m_b , is summarized in Table II and also displayed in Fig. 5. The value of m^*/m_b is almost equal to 3.1 though increases gradually and systematically as we decrease the Sr content x .

As already described, the large buckling of the V-O-V bond angle in going from SrVO_3 to CaVO_3 (in CaVO_3 $\angle \text{V-O-V} \sim 160^\circ$, which is almost equal to the insulating $3d^1$ system LaTiO_3) can lead this system closer to the boundary of the MI transition. Actually, a significant spectral weight redistribution, which is a manifestation of a strong electron correlation, has been observed al-

ready in this system.¹⁹⁻²² Nevertheless, no significant amount of mass-enhancement can be deduced from this magnetic measurement. This surprising result motivates us to reconsider whether this system may indeed be a correlated metallic system. However, as well as the reported spectral weight redistribution, the measurement of the electronic specific heat and electric resistivity described below give us further evidence of strong correlations in this system.

C. Electronic specific heat coefficient

An alternative method to evaluate m^* is to measure the electronic contribution to the specific heat, γT , which reflects DOS at E_F . γ is called the electronic specific heat coefficient. Using $D(E_F)$ Ryd⁻¹formula-unit⁻¹ obtained by the LDA band calculation, we can deduce the value of electronic specific heat coefficient in the non-interacting limit γ^{LDA} :

$$\gamma^{LDA} = \frac{\pi^2}{3} k_B^2 N D(E_F),$$

where N is the number of itinerant electrons per mole in the unit formula. Then,

$$\gamma^{LDA} [\text{mJ/molK}^2] = 0.173238 \times D(E_F).$$

The ratio of the effective mass to the band mass (m^*/m_b) is deduced from the ratio of the observed γ to the calculated γ^{LDA} .

Sufficiently below the Debye temperature Θ , the constant volume specific heat C_v/T can be plotted against T^2 , *i.e.*,

$$C_v/T = \gamma + \beta T^2 \quad (3)$$

in order to separate out the contribution of the ionic degrees of freedom (βT^3) dominant at high temperatures. The coefficient β is related to Θ as follows:

$$\begin{aligned} \beta &= \frac{9Nk_B}{\Theta^3} \int_0^{\Theta/T} \frac{e^z z^4 dz}{(e^z - 1)^2} \\ &\simeq \frac{12\pi^4 Nk_B}{5\Theta^3} (T \ll \Theta). \end{aligned}$$

Here we note that experiments measure the specific heat at constant pressure, C_p , but we normally compare this result to C_v , since these two are almost identical in a solid.

The measured constant pressure specific heats C_p of $\text{Ca}_{1-x}\text{Sr}_x\text{VO}_3$ below ~ 15 K are shown in Fig. 6. In the temperature range displayed in Fig. 6, it is clear that the data do not behave simply as Eq. 3. Thus, we have tried to fit the data to Eq. 3 below $T^2 < 2 \times 10^2 \text{ K}^2$ ($T < \sim 14$ K), where the identity seems more applicable.³⁴ All the results of the least-square fits are summarized in Table III. We find that the value of γ , even in CaVO_3 ($x = 0$), is still not so enhanced as we discuss below ($m^*/m_b \simeq 2$), although these values are comparable to the $\text{La}_{1-x}\text{Sr}_x\text{TiO}_3$ system in the La rich phase except for $x < 0.05$. (The

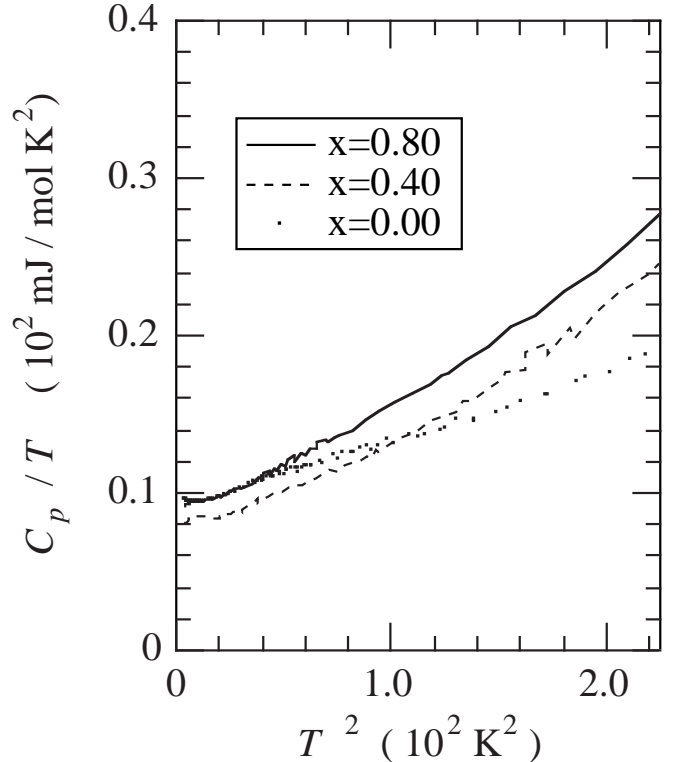


FIG. 6. Specific heat of poly-crystalline $\text{Ca}_{1-x}\text{Sr}_x\text{VO}_3$ divided by T plotted against T^2 .

γ values in the $\text{Ca}_{1-x}\text{Sr}_x\text{VO}_3$ system are much larger than that of the less correlated sodium metal $\sim 1 \text{ mJ mol}^{-1}\text{K}^{-2}$.) The obtained Debye temperatures Θ are comparable to $\Theta \sim 300$ K deduced from the temperature of the phonon-drag peak of the Seebeck coefficient of CaVO_3 ,³⁵ substantiating the result of our least-square fit to the specific heat data.

The effective masses compared to the band masses m^*/m_b are defined as the ratios of the observed γ to the γ^{LDA} . We plot the values of m^*/m_b against x with those deduced from the magnetic susceptibilities for comparison (Fig. 7).

From Fig. 7, we can also estimate the Sommerfeld-Wilson's ratio R_W :³⁶

$$R_W \equiv \frac{\gamma^{LDA}}{\chi_P^{LDA}} \frac{\chi_P}{\gamma} = \frac{\left(\frac{m^*}{m_b}\right)_\chi}{\left(\frac{m^*}{m_b}\right)_\gamma}$$

It is worthwhile emphasizing that R_W is of order unity, implying that the electronic specific heat coefficient γ is similarly enhanced to the Pauli paramagnetic susceptibility χ_P . Furthermore, this means it is appropriate to assume a one-to-one correspondence between the quasi-particle excitations of this system and those of a free-electron gas.

For a non-interacting Bloch-electron system, $R_W = 1$. One of the possible reasons for $R_W \neq 1$ is a ferromagnetic fluctuation, which enters in χ_P as $\chi_P/\chi_P^0 = (m^*/m_o)S$, where $S = (1 + F_o^a)^{-1}$ is called the Stoner enhancement

TABLE III. Fitted parameters for the specific heat and deduced effective mass m^* of $\text{Ca}_{1-x}\text{Sr}_x\text{VO}_3$. γ^{LDA} has been calculated from $D(E_F)$ obtained by the LDA band calculation³⁰ with a simple scaling correction obtained by multiplying each value by $1/\cos^2(\angle\text{V-O-V})$ which accounts for the narrowing of the band due to the buckling. m^*/m_b is defined as the ratio between γ and γ^{LDA} .

x	Θ (K)	γ (mJ mol ⁻¹ K ⁻²)	γ^{LDA} (mJ mol ⁻¹ K ⁻²)	m^*/m_b
0.00	368.0	9.248	4.475	2.067
0.20	348.3	7.554	4.391	1.720
0.40	320.6	7.123	4.307	1.654
0.80	300.0	8.239	4.223	1.951
1.00	322.4	8.182	4.134	1.979

factor including the 0-th asymmetric Landau parameter F_o^a . (For an isotropic free-electron system, R_W becomes unity, because $F_o^a = 0$.) In exchange-enhanced metals, *i.e.*, a system with ferromagnetic fluctuations, S plays an important role and R_W becomes fairly large. However, this is not the case for the $\text{Ca}_{1-x}\text{Sr}_x\text{VO}_3$ system, since we have not observed any traces of ferromagnetic fluctuations.

The value of R_W for $\text{Ca}_{1-x}\text{Sr}_x\text{VO}_3$ deduced from our experiments is almost 2, as illustrated in Fig. 7, where the half values of m^*/m_b deduced from the magnetic measurements are plotted for comparison. In strongly correlated electron systems, it has been argued that the value of R_W becomes equal to 2 at $U/W = \infty$.^{36,37} Although there is a small deviation, $R_W \approx 2$ clearly indicates the importance of electron correlations in this system.

In order to explain the deviation from $R_W = 2$, we assume that the shaded area in Fig. 7 corresponds mainly to the contribution of the electron-phonon interaction. It is known that this interaction contributes a factor $(1 + \lambda)$ to γ , but not to χ_P . Hence, R_W is modified to become $R_W(1 + \lambda)^{-1}$. From Fig. 7, we can approximately estimate $\lambda < \sim 0.3$, so that the electron-phonon interaction in this system is fairly small. In addition, it should be noted that, for the higher orbital degeneracies, R_W decreases towards unity in the limit of large orbital degeneracy.³⁸ Since the degeneracies of the t_{2g} orbitals of the vanadium 3d electrons are not completely released in this $\text{Ca}_{1-x}\text{Sr}_x\text{VO}_3$ system, we believe that the shaded area is not only due to the small contribution of the electron-phonon interaction but also due to the orbital degeneracy.

Thus, we can safely conclude that $R_W \simeq 2$ implies that electron correlations are strong in this system. Then, the question arises why is the enhancement of the effective mass so moderate, despite the presence of such large electron correlations?

The effective mass of a quasi-particle at the Fermi energy E_F is defined in general as;

$$m^* = \left(\frac{1}{\hbar^2 \vec{k}} \frac{d\varepsilon_k}{dk} \Big|_{\vec{k}=\vec{k}_F} \right)^{-1}, \quad (4)$$

where ε_k is quasi-particle energy that is given as a solution $\omega = \varepsilon_k$ of the equation

$$\omega = \varepsilon_k^0 + \text{Re}\Sigma(\vec{k}, \omega), \quad (5)$$

where $\Sigma(\vec{k}, \omega)$ is the self-energy of the system in which all of the interaction effects are contained. ε_k^0 corresponds to the energy of a non-interacting Bloch electron. However, in this study, we regard ε_k^0 as the energy dispersion of a single-electron band obtained by the LDA band-calculation. Thereby, ε_k^0 gives a band mass m_b :

$$m_b = \left(\frac{1}{\hbar^2 \vec{k}} \frac{d\varepsilon_k^0}{dk} \Big|_{\vec{k}=\vec{k}_F} \right)^{-1}. \quad (6)$$

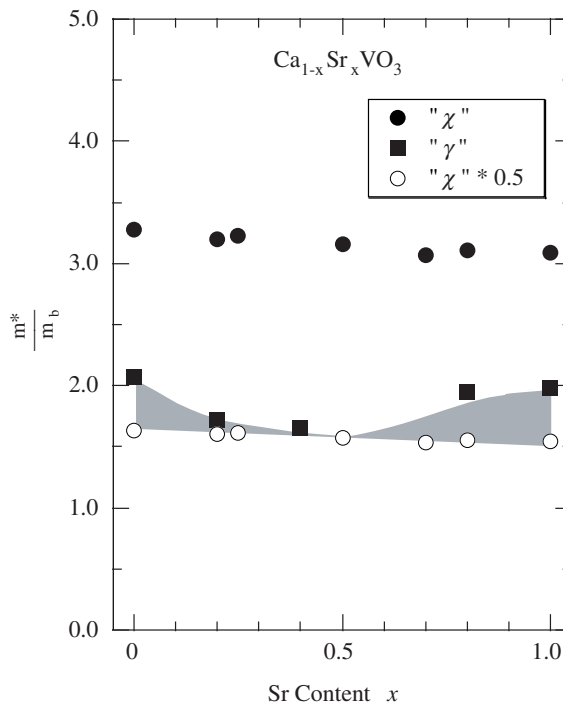


FIG. 7. Ratio of the effective mass and band mass obtained by comparing the observed γ with the calculated γ^{LDA} (filled squares, denoted by “ γ ”). “ χ ” stands for the effective mass deduced from χ_P (filled circles, denoted by “ χ ”) and the half values of “ χ ” (open circles) also plotted for comparison. The shaded area stands for the deviation from $R_W = 2$.

As is apparent from these definitions (Eqs. 4 and 6), m^* and m_b are given as tensors, but we assume here that the Fermi surface is isotropic and therefore m^* is nothing but a scalar quantity. Using Eqs. 4, 5 and 6, we deduce that the effective mass is given by the following expression:

$$\begin{aligned} \frac{m^*}{m_b} &= \frac{\left| \frac{d\varepsilon_k^0}{dk} \right|_{\vec{k}=\vec{k}_F}}{\left| \frac{d\varepsilon_k}{dk} \right|_{\vec{k}=\vec{k}_F}} \\ &= \left(1 - \frac{\partial \text{Re}\Sigma(\vec{k}, \omega)}{\partial \omega} \Big|_{\omega=E_F} \right) \\ &\quad \times \frac{\left| \frac{d\varepsilon_k^0}{dk} \right|_{\vec{k}=\vec{k}_F}}{\left| \frac{d\varepsilon_k^0}{dk} \Big|_{\vec{k}=\vec{k}_F} + \frac{\partial \text{Re}\Sigma(\vec{k}, \omega)}{\partial k} \Big|_{\vec{k}=\vec{k}_F}} \\ &\equiv \frac{m_\omega}{m_b} \times \frac{m_k}{m_b}, \end{aligned}$$

where m_ω is called “ ω -mass” and m_k is called “ k -mass”.³⁹ If we consider only the on-site Coulomb interaction as the origin of the electron correlation and average out the fluctuation of the neighboring sites as in the limit of large lattice connectivity,⁴⁰ the self-energy depends only on the quasi-particle energy ω , *i.e.*, $\Sigma(\vec{k}, \omega) \equiv \Sigma(\omega)$. Then, the effective mass becomes (since $m_k/m_b = 1$):

$$\frac{m^*}{m_b} = \left(1 - \frac{\partial \text{Re}\Sigma(\omega)}{\partial \omega} \Big|_{\omega=E_F} \right) \equiv Z^{-1},$$

where Z is the quasi-particle weight. Therefore, a critical enhancement of the effective mass due to strong electron correlations ($Z \rightarrow 0$) is inevitable at the MIT point.

However, in general, since the electron correlation is not necessarily confined to each atomic site, we may need to take into account the effect of the non-local Coulomb interaction, *i.e.*, the self-energy should have a momentum-dependence.⁴¹ Especially in the dynamical mean-field approach to the Mott transition,⁴⁰ the non-locality of the exchange interaction is not treated; therefore, we should introduce $\Sigma(\vec{k}_F, E_F)$, which is considerably different from zero.²⁰ The screening of the Coulomb potential can reduce $\Sigma(\vec{k}_F, E_F)$, because in well-screened systems such as conventional metals, the Coulomb potential is no longer long-range and the non-locality of the exchange interaction is small. However, in most of the perovskite-type TM oxides, the carrier density is fairly small, and this effect will be more significant in the vicinity of the MIT point.

We must assume therefore that, near the MIT point, the ω -mass increases significantly reflecting $Z \rightarrow 0$; on the other hand, due to poor-screening, the contribution of the momentum-dependent self-energy becomes significant, resulting in a decrease of the k -mass. Thus, the critical enhancement of the effective mass, which is a product of the ω -mass and the k -mass, can be suppressed in some conditions.¹⁹ This is not only a plausible idea of

explaining the behavior of the effective mass but also a model which provides a desirable picture of the reduction of the spectral intensity at the Fermi energy observed in the photoemission and inverse-photoemission spectroscopies.^{19,20,42}

In summary, in order to obtain a comprehensive understanding of the metallic state near the Mott transition, we should note that the momentum-dependence of the self-energy plays an important role in this region.

D. Electric resistivity

The electric resistivities collected on both heating and cooling cycles between 350 K and 4 K show no difference within the experimental accuracy. In some cases, the resistivity shows clear dependence on the crystallographic alignments of the experiment; *i.e.*, when the measuring current flows parallel to the [100]-axis of the pseudocubic perovskite, the resistivity is different from that when the current flows along the [110]-axis. This anisotropy, however, is not temperature-dependent. Whenever we observe such anisotropy, we normalize each data set to the residual resistivity ρ_0 , and the resulting curves fit each other completely.

The scaling factor $c \equiv \rho^{[110]}(T)/\rho^{[100]}(T)$, varies from ~ 1.1 to ~ 1.5 . However there seems to be neither a systematic relation between c and the Sr content x , nor consistency among the different sets of the measurements for the samples with the same value of x .

Thus, we consider that the observed anisotropy is not due to any particular feature of the electronic structure of the system. Similar behavior has been reported in the resistivity of the single crystal CoSi_2 with cubic C1 structure,⁴³ and also high-purity cubic Al single crystal.⁴⁴ In the former material, it was pointed out that the anisotropy can be attributed to an extrinsic origin, *e.g.*, point defects and/or dislocations that appeared during crystal growth, though no trace of such defects has yet been observed.⁴³ It has been argued that, in the case of the Al single crystal, a model calculation for $\langle 211 \rangle$ dislocations predicts an anisotropy of electrical resistivity compatible with experiment.⁴⁵ Therefore, we suggest that the anisotropy in our resistivity measurements may also be caused by the presence of a small amount of defects and/or dislocations.⁴⁶ Despite this undesirable artifact, if we make the size of the rectangular parallelepiped as small as $2 \times 0.5 \times 0.3 \text{ mm}^3$, the absolute values of the electric resistivity data can be reproduced within the $\pm 15\%$ error bar (the temperature dependence is completely reproducible as mentioned above) irrespective of the direction of the measuring current. With all these considerations, the data were collected as shown in Fig. 8.

At first sight, all the data seem to be well expressed by the relation $\rho = \rho_0 + AT^2$ for the measured temperature range. However, when we try to fit the observed resistivity using this expression, we cannot fit the data over the entire temperature range from 4 K to 350 K using a single value of the coefficient A . Therefore we assume that the

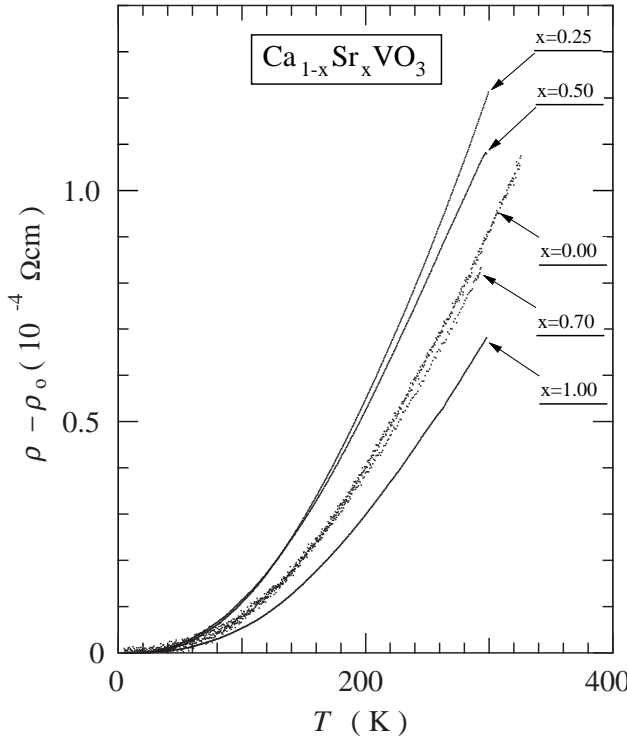


FIG. 8. Electric resistivities of the $\text{Ca}_{1-x}\text{Sr}_x\text{VO}_3$ single crystals for $x = 0.00, 0.25, 0.50, 0.70, 1.00$. For each data set, the minimum resistivity at $\sim 4\text{ K}$ has been subtracted as the residual resistivity ρ_o .

resistivity is expressed by $\rho_o + AT^2$ plus an *additional term*.

Firstly, we consider here that the AT^2 term is due to electron-phonon scattering. It has been suggested, especially in strongly-coupled superconductors, that the AT^2 term is due to the breakdown of the momentum-conservation law in the electron-phonon scattering process.⁴⁷ Here the coefficient A is shown to be related to both the residual resistivity ρ_o and the Debye temperature Θ :

$$A = \alpha \times \frac{\rho_o}{\Theta^2} \quad (7)$$

with α varying from ~ 0.01 to ~ 0.1 . However, the A values in the $\text{Ca}_{1-x}\text{Sr}_x\text{VO}_3$ system, which are roughly estimated as $\sim 1 \times 10^{-9} \Omega\text{cm}/\text{K}^2$, are three orders larger than

$$\begin{aligned} \alpha \times \frac{\rho_o}{\Theta^2} &= \alpha \times \frac{\sim 1 \times 10^{-5} (\Omega\text{cm})}{(\sim 5 \times 10^2)^2 (\text{K}^2)} \\ &= \sim 4 \times 10^{-12} (\Omega\text{cm}/\text{K}^2), \end{aligned}$$

even if we assume the largest value of $\alpha \sim 0.1$. (Here we used the Debye temperature estimated from the specific heat measurement.) Furthermore, Gurvitch has discussed that a strong electron-phonon interaction is insufficient for the T^2 law; the simultaneous presence of strong coupling and disorder is also necessary.⁴⁸ He has also pointed out that, in some cases, Eq. 7 is not applicable;

i.e., there is an empirical condition for the appearance of the T^2 law:

$$(\lambda - 0.7) \times \rho_o > \sim 13 (\mu\Omega\text{cm}),$$

where λ is the electron-phonon coupling constant. In the $\text{Ca}_{1-x}\text{Sr}_x\text{VO}_3$ system, however, λ is at largest ~ 0.3 as discussed in Sec. IIIC, and ρ_o is $\sim 1 \times 10^{-5} \Omega\text{cm}$. Hence, the last formula is not satisfied. (In the first place, even the value of λ is smaller than 0.7.) Following these arguments, it appears unlikely that the T^2 -dependent resistivity in $\text{Ca}_{1-x}\text{Sr}_x\text{VO}_3$ arises from electron phonon scattering. However, this kind of contribution to the T^2 term is not completely neglected and will be discussed again below.

An alternative and more likely origin of the T^2 term is electron-electron scattering in the presence of the umklapp process. Let us consider here the resistivity as modeled by a three-component expression of the form:

$$\rho = \rho_o + \rho_{e-e}(T) + \rho_{e-ph}(T)$$

where ρ_o is a temperature-independent background contribution due to static disorder, $\rho_{e-e}(T) \equiv AT^2$ is the electron-electron scattering. By the line-shape analysis such as is shown in Fig. 9, we found that the third term $\rho_{e-ph}(T)$ is well represented by the classical Bloch-Grüneisen formula for electron-phonon scattering with $n = 5$, developed for an isotropic Fermi surface and a simple phonon spectrum:

$$\rho = \rho_o + AT^2 + \frac{4\kappa T^n}{\Theta^6} \int_0^{\Theta/T} \frac{e^z z^n dz}{(e^z - 1)^2} \quad (n = 5) \quad (8)$$

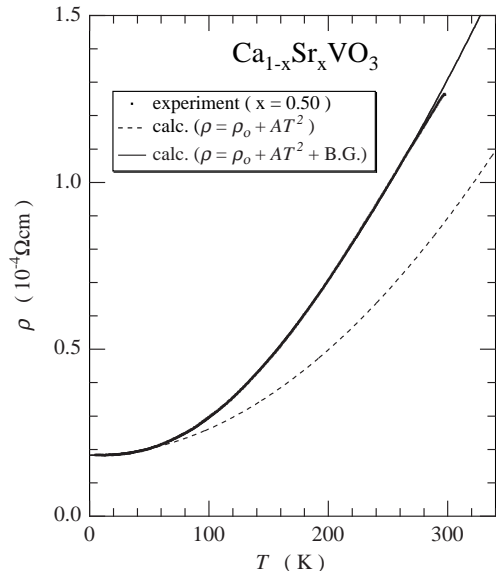


FIG. 9. Electric resistivity of $\text{Ca}_{0.5}\text{Sr}_{0.5}\text{VO}_3$ against temperature T (dots). The solid line represents Eq. 8, while the broken line represents Eq. 8 without the Bloch-Grüneisen term.

We have done a least-square fit to all the data using Eq. 8 and the obtained parameters are summarized in Table IV and also in Fig. 10. If we accept $\sim \pm 15\%$ error

TABLE IV. Fitted parameters for the electric resistivity of $\text{Ca}_{1-x}\text{Sr}_x\text{VO}_3$ with Eq. 8.

x	ρ_o (Ωcm)	A ($(\Omega\text{cm}/\text{K}^2)$)	κ ($\Omega\text{cm K}$)	Θ (K)
0.00	8.668×10^{-6}	5.911×10^{-10}	0.114	793.5
0.25	1.319×10^{-5}	9.118×10^{-10}	9.476×10^{-2}	722.2
0.50	1.827×10^{-5}	7.900×10^{-10}	7.441×10^{-2}	647.3
0.70	8.656×10^{-6}	6.796×10^{-10}	8.073×10^{-2}	811.5
1.00	6.205×10^{-6}	4.208×10^{-10}	0.121	866.3

bar, we can conclude that each of the fitted parameters shows systematic behavior as a function of Sr content x .

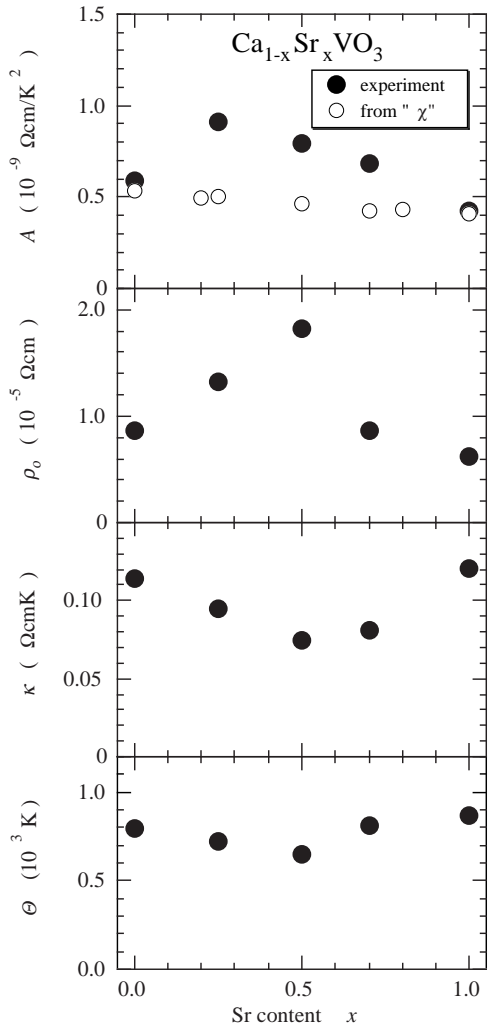


FIG. 10. Fitted parameters for the electric resistivity: A , ρ_o , κ and Θ in Eq. 8, plotted against Sr content x . The A values deduced from the Pauli paramagnetic susceptibility under the assumption of $R_W = 2$ and the Kadowaki-Woods ratio is $1.0 \times 10^{-5} \mu\Omega\text{cm mol K (mJ)}^{-2}$ are also plotted for comparison (top).

ρ_o shows a maximum at $x = 0.5$. This reflects that the system has the maximum amount of randomness at that composition.

We note that our effective transport Debye temperature $\Theta \sim 700\text{K}$ does not sound physical. However it is

not necessary for the transport Θ to be equal to the thermodynamic value $\Theta \sim 350\text{K}$ obtained from the specific heat measurements. This is because the transport Debye temperature involves only the acoustic modes that interact with the electrons, whereas the thermodynamic Debye temperature considers all types of phonons.⁴⁹

The values of κ and Θ show a minimum at $x = 0.5$, indicating that the lattice becomes softest at this composition. The electron-phonon coupling constant λ is related to both κ and Θ as follows:

$$\lambda \propto \frac{\omega_p^2}{\Theta^2} \kappa,$$

where ω_p is the plasma frequency of the conduction electrons. Makino *et al.* reports in the following paper²² that the variation of ω_p in going from SrVO_3 to CaVO_3 is systematic but very small, and the variation of λ inferred from the Sommerfeld-Wilson's ratio R_W is also small. Thus we can roughly estimate that $\kappa \sim \Theta^2$. This is consistent with the behaviors shown in Fig. 10.

It is surprising that the contribution of the electron-electron scattering, which is in general dominant at very low temperature, is significantly large even at room temperature. In $\text{Ca}_{0.5}\text{Sr}_{0.5}\text{VO}_3$,

$$\rho_{e-e}(300\text{K}) : \rho_{e-ph}(300\text{K}) \sim 2 : 1.$$

This is further evidence that the electron correlations are significantly large in this system. The coefficient A should, then, reflect the enhancement of the effective mass of the quasi-particles due to this electron correlation. The resistivity due to electron-electron (*i.e.*, quasi-particle – quasi-particle) scattering can be crudely but quantitatively expressed as follows:

$$\begin{aligned} \rho_{e-e}(T) &= \frac{m_b}{ne^2\tau} \\ &= \frac{m^*v_F}{e^2n^{2/3}} \left(\frac{k_B T}{E_F} \right)^2 \\ &= \frac{4k_B^2 m^{*2}}{\hbar^3 e^2 n^{2/3} k_F^3} T^2 \\ &\equiv AT^2, \end{aligned}$$

where $v_F = \hbar k_F/m^*$, $E_F = \hbar^2 k_F^2/(2m^*)$, and we have assumed the scattering time τ is equal to the life time of the thermally activated quasiparticle $\tau^{-1} = v_F n^{1/3} E_F^{-1} Z^{-1} \text{Im} \Sigma \simeq v_F n^{1/3} (m^*/m_b) (k_B T/E_F)^2$.⁵⁰ Hence, the coefficient A is proportional to the quadratic of the effective mass m^* . The obtained value of A increases systematically in going from $x = 1$ to $x = 0.25$;

this may correspond to the increase of m^* . However there seems to be a rapid decrease between $x = 0.25$ and $x = 0$ which is not consistent with the behavior of m^* . This is not obviously explained by the considerably large error arising from the quality of the sample ($\sim \pm 15\%$).

In Fig.10 (top), we also plot the value of A deduced from the Pauli paramagnetic susceptibility χ_P under a few reasonable assumptions: we use a Sommerfeld-Wilson's ratio $R_W = 2$ to estimate the electronic specific heat γ from χ_P , since R_W is almost equal to 2 in this system. The obtained γ corresponds to the electronic specific heat which is not affected by the electron-phonon interaction. Then we use the Kadowaki-Woods ratio A/γ^2 , which is a measure of the electron correlation, of the same value as that of the heavy fermion systems,⁵¹ *i.e.* $A/\gamma^2 = 1.0 \times 10^{-5} \mu\Omega \text{ cm mol K (mJ)}^{-2}$, and deduced the value of A . The resulting A values are compared to the experimentally observed values (Fig. 10, top).

Since the above assumptions for the Sommerfeld-Wilson's ratio and the Kadowaki-Woods ratio in this system seem to be fairly appropriate, we can safely say that the AT^2 term in the resistivity of the end members CaVO_3 ($x = 0$) and SrVO_3 ($x = 1$) is attributed to only the electron-electron scattering. For the other solid-solutions ($0 < x < 1$), there must be other contributions to the AT^2 term. The most probable candidate of this additional contribution of the T^2 term is the interference between the elastic electron scattering and the electron-phonon scattering, which has been recently investigated by Ptitsina *et al.*⁵² This effect must be proportional to the residual resistivity, and our data seems to support the scenario.

On the other hand, however, we know that the Kadowaki-Woods ratio is not necessarily equal to the above value. Then, there are several other reasons to be considered for the observed x -dependence of A . We must consider a possible contribution from the modification of the Fermi surface. Since A is not only proportional to $m^*{}^2$ but also to $k_F{}^{-3}$, a variation of the shape of the Fermi surface due to the orthorhombic distortion may lead to changes in A . In passing, as we apply pressure to CaVO_3 , the value of A tends to decrease,^{35,53} though it has not yet been determined how the lattice constants change under pressure. We should also remark that samples around $x = 0.25$ have a tendency to show the smallest spectral weight at the Fermi energy as observed in the recent studies of the photoemission spectroscopy⁵⁴ and the inverse photoemission spectroscopy of the $\text{Ca}_{1-x}\text{Sr}_x\text{VO}_3$ single crystals.⁵⁵ This might be related to the hybridization between the V 3d t_{2g} orbitals and the O 2p σ orbitals. Okimoto *et al.* calculated a distortion-induced admixture between those orbitals,⁵⁶ and Lombardo *et al.* discussed a possible scenario involving spectral weight transfer in the $\text{Ca}_{1-x}\text{Sr}_x\text{VO}_3$ system due to charge transfer.⁵⁷ This distortion-induced charge transfer may explain the strange revival of the quasi-particle weight in the region

* Electronic address: INOUE@ETL.GO.JP

close to CaVO_3 , and this hybridization may also explain the x -dependence of the value of A , although this should be consistent with the monotonic increase of the effective mass toward CaVO_3 as estimated from the Pauli paramagnetism. Finally, the contribution of the momentum-dependence of the self-energy, which becomes significant in the region closer to CaVO_3 ,^{19,20} is also an intriguing candidate to explain the behavior of A . Apparently, with a large momentum-dependence of the self-energy, it is no longer necessary that A is proportional to $m^*{}^2$. These issues will be clarified by further investigations.

IV. SUMMARY AND CONCLUDING REMARKS

We have succeeded to prepare single crystals of the metallic alloy system $\text{Ca}_{1-x}\text{Sr}_x\text{VO}_3$ for the first time, as far as we are aware. The system has nominally one 3d electron per vanadium ion; as we substitute a Ca^{2+} ion for a Sr^{2+} ion, the band width W decreases due to the buckling of the V-O-V bond angle from $\sim 180^\circ$ for SrVO_3 to $\sim 160^\circ$ for CaVO_3 , which is almost equal to the analogous 3d¹ insulator LaTiO_3 . Thereby, it is reasonable to consider that CaVO_3 is close to the boundary of MIT. The Sommerfeld-Wilson's ratio $R_W \simeq 2$, the Kadowaki-Woods ratio A/γ^2 lie in the same region as the heavy Fermion compounds, and there is a large contribution from electron-electron scattering to the resistivity even at room temperature. These features are considered to provide strong evidence of the large electron correlations in this system. However, the effective masses obtained by the thermodynamic (γ) and magnetic (χ_P) measurements show only a moderate increase in going from SrVO_3 to CaVO_3 , instead of the diverging behaviors expected from the Brinkmann-Rice picture.

The elaborate band-width control in $\text{Ca}_{1-x}\text{Sr}_x\text{VO}_3$ has elucidated that the mass-enhancement due to the reduction of the band width is not so large, even though the system shows some fingerprints of a large electron correlation. Accordingly, we suggest that these seemingly contradicting metallic properties observed in this system can be explained by considering the effect of non-local electron correlations, *i.e.*, the momentum-dependent self-energy.

V. ACKNOWLEDGEMENT

We would like to thank A. Fujimori, M. J. Rozenberg, A. Yoshimori, H. Bando, N. Shirakawa, and I. Hase for many fruitful and stimulating discussions. We also thank Y. Ueda for showing the data of the crystal structure of CaVO_3 before the publication. Finally, we gratefully acknowledge many experimental supports and suggestions, at various stages of this work, by Y. Nishihara, K. Oka, F. Iga, H. Kawanaka, A. Fukushima, T. Ito, Y. Kodama and other members of Electron Physics group in Electrotechnical Laboratory.

[†]Present Address: Electrotechnical Laboratory, Tsukuba 305-8568, Japan.

[‡]Present Address: CREST Fellow, Institute for Solid State Physics, University of Tokyo, 7-22-1 Roppongi, Minato-ku, Tokyo 106, Japan

¹For a concise review, see A. Fujimori and T. Mizokawa, *Current Opinion Solid State Mater. Sci.* **2**, 18 (1997).

²R. E. Peierls, in *Proc. Phys. Soc.* **A49**, (1937).

³N. F. Mott, *Proc. Phys. Soc.* **A62**, 416 (1949).

⁴For a recent review, see *Spectroscopy of Mott Insulator and Correlated Metals*, edited by A. Fujimori and Y. Tokura (Springer-Verlag, Berlin, 1995).

⁵Y. Tokura, Y. Taguchi, Y. Okada, Y. Fujishima, T. Arima, K. Kumagai, and Y. Iye, *Phys. Rev. Lett.* **70**, 2126 (1993).

⁶F. Lichtenberg, D. Widmer, J. G. Bednorz, T. Williams, and A. Reller, *Z. Phys.* **B82**, 211 (1991); D. A. Crandles, T. Timusk, and J. E. Greedan, *Phys. Rev. B* **44**, 13250 (1991); D. A. Crandles, T. Timusk, J. D. Garrette, and J. E. Greedan, *Physica C* **201**, 407 (1992).

⁷W. F. Brinkman and T. M. Rice, *Phys. Rev. B* **2**, 4302 (1970).

⁸T. Katsufuji and Y. Tokura, *Solid State Phys.* **30**, 15 (1995), in Japanese; Y. Okada, Master Thesis (Univ. of Tokyo, 1993), unpublished.

⁹Y. Tokura, Y. Taguchi, Y. Moritomo, K. Kumagai, T. Suzuki, and Y. Iye, *Phys. Rev. B* **48**, 14063 (1993).

¹⁰F. Iga, Y. Nishihara, J. Sakurai, and M. Ishikawa, *Physica B* **237-238**, 14 (1997).

¹¹D. B. McWhan, A. Menth, J. P. Remeika, W.F. Brinkman, and T. M. Rice, *Phys. Rev. B* **7**, 1920 (1973); S.A. Carter, T. F. Rosenbaum, P. Metcalf, J. M. Honig, and J. Spalek, *ibid.* **48**, 16841 (1993); S.A. Carter, T. F. Rosenbaum, M. Lu, H. M. Jaeger, P. Metcalf, J. M. Honig, and J. Spalek, *ibid.* **49**, 1378 (1994).

¹²J. B. Torrance, P. Lacorre, A. Lacorre, A. I. Nazzal, E. J. Ansaldo, and Ch. Niedermayer, *Phys. Rev. B* **45**, 8209 (1992); X. Granados, J. Fontcuberta, X. Obarados, and J. B. Torrance, *ibid.* **46**, 15683 (1992); X. Obarados, L. M. Paulis, B. Maples, J. B. Torrance, A. I. Nazzal, J. Fontcuberta, and Y. Granados, *ibid.* **47**, 12353 (1993); P. C. Canfield, J. D. Thompson, S. -W. Cheong, and L. W. Pupp, *ibid.* **47**, 12357 (1993); J. L. García-Muñoz, J. Rodríguez-Carvajal, and P. Lacorre, *ibid.* **50**, 978 (1994); T. Arima and Y. Tokura, *J. Phys. Soc. Jpn.* **64**, 2488 (1995).

¹³J. A. Wilson and G. D. Pitt, *Phil. Mag.* **23**, 1297 (1971); G. Czyzak, J. Fink, H. Schmidt, G. Krill, M. F. Lapierre, P. Paissod, F. Gautier, and C. Robert, *J. Mag. Mag. Mat.* **3** 58 (1976); S. Ogawa, *J. Appl. Phys.* **50**, 2308 (1979); H. Takagi, H. Eisaki, S. Uchida, and R. J. Cava, in Ref. 4, p. 185; Y. Sekine, H. Takahashi, N. Môri, T. Matsumoto, and T. Kosaka, *Physica B* **237-238**, 148 (1997).

¹⁴J. Zaanen, G.A. Sawatzky, and J.W. Allen, *Phys. Rev. Lett.* **55**, 418 (1985).

¹⁵S. Hüfner, *Z. Phys. B* **61**, 135 (1985).

¹⁶M. Marezio, J. P. Remeika, and P. D. Dernier, *Acta Crystallogr. B* **26**, 2008 (1970); D. A. MacLean, Hok-Nam Ng, and J.E. Greedan, *J. Solid State Chem.* **30**, 30 (1979).

¹⁷R. D. Shannon, *Acta Crystallogr. A* **32**, 751 (1976).

¹⁸The GdFeO_3 type lattice distortion possibly causes anisotropy and affects electron-phonon interactions. However, in this system, these contributions are not predominant for the metallic properties, as revealed by our measurements and the following discussion. This could also justify the metallic $\text{Ca}_{1-x}\text{Sr}_x\text{VO}_3$ alloy is an ideal compounds.

¹⁹I. H. Inoue, I. Hase, Y. Aiura, A. Fujimori, Y. Haruyama, T. Maruyama, and Y. Nishihara, *Phys. Rev. Lett.* **74**, 2539 (1995).

²⁰K. Morikawa, T. Mizokawa, K. Kobayashi, A. Fujimori, H. Eisaki, S. Uchida, F. Iga, and Y. Nishihara, *Phys. Rev. B* **52**, 13711 (1995).

²¹M. J. Rozenberg, I. H. Inoue, H. Makino, F. Iga, and Y. Nishihara, *Phys. Rev. Lett.* **76**, 4781 (1996).

²²H. Makino, S. Onari, and I. H. Inoue, following paper, *Phys. Rev. B* (submitted).

²³I. H. Inoue, K. Morikawa, H. Fukuchi, T. Tsujii, F. Iga, and Y. Nishihara, *Jpn. J. Appl. Phys.* **32**, 451 (1993).

²⁴Very recently, we have obtained preliminary specific heat data for single crystals, which are almost similar to those for the poly crystals.

²⁵M. Ishikawa, Y. Nakazawa, T. Takabatake, A. Kishi, R. Kato, and A. Maesono, *Solid State Comm.* **66**, 201 (1988).

²⁶Y. Ueda, private communication.

²⁷J. C. Phillips, *Phys. Rev. B* **46**, 8542 (1992).

²⁸A. Fukushima, F. Iga, I. H. Inoue, K. Murata, and Y. Nishihara, *J. Phys. Soc. Jpn.* **63**, 409 (1994).

²⁹N. Shirakawa, K. Murata, H. Makino, F. Iga, and Y. Nishihara, *J. Phys. Soc. Jpn.* **64**, 4824 (1995).

³⁰In the band calculation, it is assumed that CaVO_3 has an ideal (simple-cubic) perovskite-type structure with the space group of $P_{m3m}(\text{O}_h^1)$: K. Takegahara, *J. Electron Spectrosc. Relat. Phenom.* **66**, 303 (1994); I. Hase, private communication.

³¹J. H. Van Vleck, in *The Theory of Electronic and Magnetic Susceptibilities* (Oxford University Press, United Kingdom, 1932).

³²H. Kontani and K. Yamada, *J. Phys. Soc. Jpn.* **65**, 172 (1996).

³³J. P. Pouget, H. Launois, T. M. Rice, P. Derrier, A. Gossard, G. Villeneuve and P. Hagenmuller, *Phys. Rev. B* **10**, 1801 (1974).

³⁴A bump which appears around 2 K in the specific heat can be subtracted by assuming Schottky contribution of $\sim 0.2\%$ impurities. This amount of impurities is consistent with that deduced from the magnetic Curie-Weiss contribution.

³⁵J. -S. Zhou and J. B. Goodenough, Phys. Rev. B **54**, 13393 (1996).

³⁶K. Wilson, Rev. Mod. Phys. **47**, 773 (1975).

³⁷P. Nozières, J. Low Temp. Phys. **17**, 31 (1974).

³⁸A. Yoshimori, Prog. Theor. Phys. **55**, 67 (1976).

³⁹H. R. Glyde, S. I. Hernadi, Phys. Rev. B **28**, 141 (1983); C. W. Greeff, H. R. Glyde, and B. E. Clements, *ibid* **45**, 7951 (1992).

⁴⁰For example, the Hubbard model in the limit of large lattice connectivity: A. Georges, G. Kotliar, W. Krauth, and M. J. Rozenberg, Rev. Mod. Phys. **68**, 13 (1996), and the references therein.

⁴¹Even in the case where only the on-site Coulomb interaction is included in the model Hamiltonian, the self-energy can be non-local (momentum-dependent). For example, the effect of antiferromagnetic fluctuation due to Fermi surface nesting has already been discussed in the literature: A. Kampf and J. R. Schrieffer, Phys. Rev. B **41**, 6399 (1990); M. Langer, J. Schmalian, G. Grabowsky, and K. H. Bennemann, Phys. Rev. Lett. **75**, 4508 (1995); J. J. Deisz, D. W. Hess, and J. W. Serene, Phys. Rev. Lett. **76**, 1312 (1996).

⁴²A. Fujimori, K. Morikawa, T. Mizokawa, T. Saitoh, M. Nakamura, Y. Tokura, I. Hase, and I. H. Inoue, in Ref. 4, p. 174.

⁴³T. Hirano and M. Kaise, J. Appl. Phys. **68**, 627 (1990).

⁴⁴E. Hashimoto, Y. Ueda, H. Tamura, and T. Kino, J. Phys. Soc. Jpn. **62**, 4178 (1993).

⁴⁵B. R. Watts, J. Phys. F **17**, 1703 (1987).

⁴⁶When the rate of crystal growth is fairly large, it is hard to explain this process on a plane by plane basis. However, if the crystal contains a screw dislocation, it is never necessary to nucleate a new plane, as the local planar structure can wind endlessly about the screw dislocation. This kind of process might be realized in some cases during our crystal growth.

⁴⁷S. Koshino, Prog. Theor. Phys. **24**, 1049 (1960); *ibid* **30**, 415 (1963); P. L. Tayler, Phys. Rev. **135**, A1333 (1964); Yu. Kagan and A. P. Zhernov, Zh. Eksp. Teor. Fiz. **50**, 1107 (1966); D. H. Damon, M. P. Mathur, and P. G. Klemens, Phys. Rev. **176**, 876 (1968); H. Takayama, Z. Phys. **263**, 329 (1973); P. J. Cote and L. V. Meisel, Phys. Rev. Lett. **39**, 102 (1977); F. J. Ohkawa, J. Phys. Soc. Jpn. **44**, 1105 (1978).

⁴⁸M. Gurvitch, Phys. Rev. Lett. **56**, 647 (1986).

⁴⁹B. Bucher, P. Steiner, J. Karpinski, E. Kaldis, and P. Wachter Phys. Rev. Lett. **70**, 2012 (1993).

⁵⁰In strongly correlated electron systems, the electron-electron scattering is the dominant process to induce the decoherence of the wavefunction, which thus determines the relaxation time τ under the presence of the umklapp process. Then, the quasi-particle – quasi-particle scattering time is given by $\tau^{-1} \propto Z^{-1} \text{Im}\Sigma$, where Z is the quasi-particle weight and Σ is the self-energy.

⁵¹K. Kadowaki and S. B. Woods, Solid State Commun. **58**, 507 (1986).

⁵²N. G. Ptitsina, G. M. Chulkova, K. S. Il'in, A. V. Sergeev, F. S. Pochinkov, E. M. Gershenson, and M. E. Gershenson, Phys. Rev. B **56**, 10089 (1997), and the references therein.

⁵³When we apply a hydrostatic pressure up to 8 GPa to CaVO₃, the resistance at room temperature decreases $\sim 30\%$ monotonically: F. Iga, unpublished.

⁵⁴I. H. Inoue, H. Makino, I. Hase, Y. Aiura, Y. Haruyama, and Y. Nishihara, Physica B **230-232**, 780 (1997).

⁵⁵D. D. Sarma and K. Maiti, private communication.

⁵⁶Y. Okimoto, T. Katsufuji, Y. Okada, T. Arima, Y. Tokura, Phys. Rev. B **51**, 9581 (1995).

⁵⁷P. Lombardo, J. Schmalian, M. Avignon, K. H. Bennemann, Physica B **230-232**, 415 (1997).